An Experimental and Theoretical Study of the O(^1D) + HD Reaction

Dianailys Nuñez-Reyes,[a,b] Kevin M. Hickson,[a,b,*] Pascal Larrégaray,[a,b] Laurent Bonnet,[a,b] Tomás González-Lezana,[c,*] Somnath Bhowmick[d,*] and Yury V. Suleimanov[d,e]

[a]*Université de Bordeaux, Institut des Sciences Moléculaires, F-33400 Talence, France*

[b]*CNRS, Institut des Sciences Moléculaires, F-33400 Talence, France*

[c]*Instituto de Física Fundamental, CSIC, IFF-CSIC Serrano 123, 28006 Madrid*

[d]*Computation-based Science and Technology Research Center, Cyprus Institute, 20 Kavafi Str., Nicosia 2121, Cyprus*

[e]*Department of Chemical Engineering, Massachusetts Institute of Technology, 77 Massachusetts Ave., Cambridge, Massachusetts 02139, United States*

[1] kevin.hickson@u-bordeaux.fr

[2] t.gonzalez.lezana@csic.es

[3] s.bhowmick@cyi.ac.cy

Abstract

This work addresses the kinetics and dynamics of the gas-phase reaction between O(^1D) and HD molecules down to low temperature. Here, measurements were performed using a supersonic flow (Laval nozzle) reactor coupled with pulsed laser photolysis for O(^1D) production and pulsed laser induced fluorescence for O(^1D) detection to obtain rate constants over the 50-300 K range. Additionally, temperature dependent branching ratios (OD+H/OH+D) were obtained experimentally by comparison of the H-/D-atom atom yields with those of a reference reaction. In parallel, theoretical rate constants and branching ratios were calculated using three different techniques; mean potential phase space theory (MPPST), the statistical quantum mechanical method (SQM) and ring polymer molecular dynamics (RPMD). Although the agreement between experimental and theoretical rate constants is reasonably good, with differences not exceeding 30 % over the entire temperature range, the theoretical branching ratios derived by the MPPST and SQM methods are as much as 50 % larger than the experimental ones. These results are presented in the context of earlier work, while the possible origins of the discrepancies between experiment and theory are discussed.

1 Introduction

Oxygen atoms in their first excited state, O(^1D), are important reactive species in the chemistry of planetary atmospheres containing oxygen bearing compounds. On Earth, the UV photodissociation of stratospheric ozone produces O(^1D) with large quantum yields which reacts with hydrogen-bearing species such as H_2, H_2O and CH_4 to form hydroxyl radicals, OH.[1] In the Martian atmosphere, O(^1D) is produced by CO_2 photolysis in the vacuum ultraviolet (VUV) wavelength region below 170 nm.[2] Here, OH radicals have several sources including the reaction of O(^1D) with H_2 and act to recycle CO back to CO_2 through the OH + CO reaction, effectively maintaining the stability of the Martian CO_2 atmosphere.[3]

The dynamics of the O(^1D)+HD reaction has been investigated experimentally on numerous occasions.[4-13] For instance, product speed and angular distributions were measured in the Doppler-shift technique under crossed-beam conditions by Che and Liu at a collision energy, E_c, of 4.55 kcal mol^{-1} (0.20 eV).[8] In addition to this, the behavior of the integral cross sections (ICS) for the production of both OH+D and OD+H was analyzed up to E_c = 6 kcal mol^{-1} (0.26 eV).[9] In a different study, Hsu and Liu[10] employed a Doppler-selected time-of-flight (TOF) apparatus with the capacity for direct three-dimensional mapping in order to overcome the resolution limitations of this approach. Product translational energy distributions and differential cross sections (DCS) measured at 0.20 eV by means of this more sophisticated set up were reported. A marked forward-backward asymmetry was observed in the angular distributions for both product channels. Kopin Liu and coworkers[11] performed a detailed investigation of this isotopic variant of the O(^1D)+H_2 reaction, reporting final-state resolved DCS measured at E_c = 2.05 kcal mol^{-1} (0.09 eV). High resolution spectra for the O(^1D)+HD → OD+H reaction were measured with a Rydberg "tagging" TOF technique which allowed the determination of the OD product quantum state distributions at different scattering angles.[13] Experimental results presented in the work by Yuan *et al.*[14] were obtained with the same

approach. The authors reported the total DCS at E_c = 7.11 kJ mol^{-1} (0.07 eV) in addition to state-to-state vibrational and rotational distributions for the reaction starting with HD(v=0, j=0) in its ground state.

The H/D ratio between the two possible outcomes after the collision between HD and an X atom is usually considered as an indicator of the dynamics of the reaction. Thus, according to pioneering theoretical investigations by Muckerman[15] those processes following an abstraction mechanism are assumed to have a value for this ratio less than one, whereas H/D ratios larger than unity correspond to insertion reactions with complex-forming dynamics. Early laser induced fluorescence (LIF) investigations of the title reaction yielded a value of 1.13 ± 0.08 for the isotopic branching ratio OD/OH between the two product channels of the O(^1D)+HD reaction.[4] Later work by Talukdar & Ravishankara[16] yielded a branching ratio of 1.33 ± 0.07 at room temperature. This preference for the OD-forming product channel rather than the OH-forming pathway was also observed in the LIF results of Ref. (5) and those reported by Che and Liu at E_c = 0.20 eV.[8] Matsumi *et al.*[6] employed both LIF and resonance-enhanced multiphoton ionization (REMPI) techniques to measure isotopic branching ratios at average collision energies of 2.4 kcal mol^{-1} (0.10 eV), producing O(^1D) from the photolysis of O_3 at 248 nm, and at 3.4 kcal mol^{-1} (0.15 eV) with the photolysis of N_2O at 193 nm as the source for oxygen atoms. Values for the isotopic channel ratios OD+H / OH+D so measured were 1.5 ± 0.2 and 1.4 ± 0.2, respectively, which were not too different from those estimated from the reaction rate constant ratios k(O+H_2) / k(O+D_2).[6] The LIF experiment by Laurent *et al.*[7] reported a value of the branching ratio of 1.35 ± 0.2 at E_c = 0.14 eV. The $\Gamma_{H/D}$ isotopic ratio was also measured in the collision energy range 0-0.25 eV by Hsu *et al.*[9] in an attempt to substantiate the existence of two distinct reaction pathways for the O(^1D)+HD reaction.

Theoretical studies have revealed the strong dependence of the branching ratio with the potential energy surface (PES) employed in the calculations.[17]

Authors of the experimental investigation performed in Ref. (11) at 0.09 eV concluded that the O(^1D)+HD reaction proceeds via the formation of a short-lived intermediate water molecule that finally decays before proper energy randomization can occur. Nonstatistical asymmetry observed in the angular distributions were interpreted as a consequence of the ensemble of possible different intermediate complexes, but it was remarked that many aspects of the measured product distributions might be explained on statistical grounds. At higher energies however, excited potential energy states[18] introduce an abstraction contribution to the overall dynamics.[12, 19, 20] QCT calculations by Alagia *et al.*[19] found angular distributions showing more backward scattering for the OD product than for OH.

In previous papers, the behavior of the rate constant for both the O(^1D)+H_2 and O(^1D)+D_2 reactions at low temperature has been investigated by means of combined experimental and theoretical studies.[21-23] Kinetics measurements typically performed within the 50-296 K temperature range using a continuous supersonic flow reactor coupled with pulsed laser photolysis to produce O(^1D) and pulsed laser-induced fluorescence in the vacuum ultraviolet wavelength range for its detection were compared with theoretical calculations. In particular, rate constants obtained by means of various numerical approaches such as ring polymer molecular dynamics (RPMD), mean potential phase space theory (MPPST) and a statistical quantum mechanical (SQM) method were thus compared with the experimental values. Some of those approaches[24, 25] had been successfully tested before on the title reaction and its isotopic variants providing a fairly good description of the most relevant dynamical features. In this work we extend those preliminary studies to the case of the O(^1D)+HD reaction.

The structure of the paper is as follows: In Section 2 the experimental set up is described; the main technical details of the different theoretical methods are shown in Section 3; results are shown and discussed in Section 4 and finally conclusions are listed in Section 5.

2 Experimental Methods

A continuous flow supersonic flow reactor was employed for these experiments. This apparatus has been described in detail in previous work[26, 27] with various modifications allowing the kinetics of excited state C(^1D),[28-34] N(^2D)[35] and O(^1D)[21, 22, 33, 36-39] atom reactions and electronic quenching processes to be studied at low temperature. As the quenching of O(^1D) atoms by N_2 is fast at low and intermediate temperatures[39, 40] only Ar based Laval nozzles could be used during this investigation as the rate constants for the O(^1D) + Ar quenching reaction are two orders of magnitude smaller.[38-40] As such, temperatures of 50 K, 75 K and 127 K could be attained by using three different Laval nozzles (see Table 1 of Grondin *et al.*[39] for the nozzle characteristics), while room temperature measurements (also employing Ar as the carrier gas) were performed by lowering the flow velocity and by removing the nozzle. Ozone (O_3) was used as the source of O(^1D) atoms during these experiments. A small flow of O_2 was passed into a cell with quartz windows. The cell itself was irradiated by a continuous pen-ray mercury lamp, producing ground state O(^3P) atoms through O_2 photolysis at UV wavelengths. O_3 molecules were generated by the termolecular association reaction O(^3P) + O_2 + M $\rightarrow$ O_3 + M (where M = O_2); a process which was rendered more efficient through the use of pressures around 700 Torr. The output of the cell containing O_2 and O_3 molecules was mixed with the carrier gas flow before reaching the Laval nozzle reservoir. O(^1D) atoms were generated in situ within the cold supersonic flow by the photolysis of O_3 at 266 nm with ~23 mJ per pulse at 10 Hz. At this wavelength, the quantum yield for O(^1D) formation is 0.9.[1] To measure temperature dependent rate constants for the O(^1D) + HD reaction, O(^1D) atoms were probed directly through pulsed laser induced fluorescence in the vacuum ultraviolet wavelength range (VUV LIF). Here, O(^1D) atoms were excited through the 2p $^1D \rightarrow$ 3s ^1D transition at 115.215 nm. Tunable radiation around this wavelength was generated by a two-step procedure. The output of a 10 Hz Nd:YAG pumped dye laser around 691 nm was frequency doubled in a beta barium borate (BBO) crystal to produce a beam around 346 nm with ~ 8 mJ pulse energy. The residual

fundamental radiation was removed by two dichroic mirrors with a peak reflectance around 355 nm while the UV beam was steered and focused into a cell, allowing VUV generation through non-resonant third-order sum-frequency mixing in negative dispersive Xe.[42] A positive dispersive rare gas, Ar, was added to the cell to improve the conversion efficiency through phase matching. 75 Torr of Xe and 155 Torr of Ar were found to represent the optimal pressures for efficient generation of VUV radiation around 115 nm. For the product branching ratio measurements, H(^2S) or D(^2S) atoms were detected at 121.567 nm and 121.534 nm respectively using a similar procedure to the one described above. In this case, a mixture of Kr (210 Torr) and Ar (540 Torr) was used to generate the VUV radiation. A MgF_2 lens served as the output window of the cell to collimate and steer the VUV beam into the reactor. The cell was attached to the reactor at the level of the detection region by a 75 cm sidearm containing baffles which allowed the residual divergent UV radiation to be efficiently removed before reaching the reactor. The VUV beam crossed the supersonic flow at right angles, exciting either reagent O(^1D) atoms or products H(^2S) or D(^2S) atoms. The on-resonance fluorescence emission was collected at right angles to both the supersonic flow and the VUV beam by a solar blind photomultiplier tube (PMT). The PMT was isolated from reactive gases in the reactor by a LiF window, while the zone between this window and the PMT was evacuated to prevent absorption by atmospheric O_2. This zone also contained a LiF lens to focus the VUV emission onto the photocathode of the PMT. The PMT output signal was processed by a boxcar integration system. The delay between photolysis and probe lasers was controlled by a digital delay generator which also served to synchronize all the acquisition electronics. 30 laser shots were recorded for each time point with at least 70 time points for each temporal profile. This included at least 15 points where the probe laser fired before the photolysis laser allowing us to set the baseline level for the measured intensities.

The gases O_2 (99.999%), Ar (99.999%), N_2 (99.999%), HD (99.5%) and Xe (99.998%) were used directly from cylinders during the present experiments. Their flows were controlled by mass-flow controllers which were calibrated for each individual gas by a pressure rise at constant volume method, with the exception of HD due to the small available quantity of this gas. As previous calibrations had already demonstrated that H_2 and D_2 flows were essentially identical for any given mass-flow controller, calibration factors for H_2 were used to derive the HD flow instead.

3 Theoretical Methods

Statistical Quantum Mechanics

The SQM method has been used before to study complex-forming reactions.[24, 25, 43-45] Assuming the formation of an intermediate species between reagents and products, we can approximate the state-to-state probability as:[24]

$$\left|S^J_{vj\Omega,v'j'\Omega'}(E)\right|^2 \approx \frac{p^J_{vj\Omega}(E)\cdot p^J_{v'j'\Omega'}(E)}{\sum_{v''j''\Omega''} p^J_{v''j''\Omega''}(E)} \qquad (1)$$

Where $p^J_{vj\Omega}(E)$ is the capture probability to form the complex from the initial state at the collision energy E and for the total angular momentum J. The indexes $vj\Omega$ and $v'j'\Omega'$ are the quantum numbers for vibrational (v), rotational (j) and third component of the angular momentum (Ω) for the initial and final rovibrational states of HD, respectively. The sum in the denominator of Eq. (1) runs for all energetically open rovibrational states at the energy E for both reagent and product channels. Using the above expression for the reaction probability, it is then possible to calculate the corresponding ICS, $\sigma_{vj\,v'j'}(E)$ and then the thermal rate constant:

$$k_{vj,v'j'}(T) = \sqrt{\frac{8\beta^3}{\pi\mu}}\int_0^\infty \sigma_{vj,v'j'}(E)e^{-\beta E}EdE \qquad (2)$$

where we have defined $\beta = (k_B T)^{-1}$ and the cross sections include the 1/5 factor corresponding to the electronic partition function. The calculation of DCSs, described elsewhere,[24] requires a random phase approximation to be invoked which neglects any

information of the S matrix phase and only reduced rotation matrix elements and the probabilities shown in Eq. (1) are used.

As in our previous investigations on the O(^1D)+D_2 reaction,[22] the calculations have been performed on the ground ^{1}A' PES of Dobbyn and Knowles (DK).[46, 47] Capture probabilities of Eq. (1) are obtained with a time-independent propagation[24] under the centrifugal sudden approximation in a region defined between R_c and R_{max} with values of 1.8 Å / 2.6 Å / 1.9 Å and 26.6 Å / 43.3 Å /31.6 Å for reactants, H+OD and D+OH product channels respectively for both the HD(v=0,j=0) and HD(v=0,j=1) initial states. ICS in a collision energy range between 10^{-4} eV and 0.32 eV with variable spaced grid were calculated and then were interpolated to 25000 energy points to obtain the rate constants from Eq. (2). For the largest energies, partial waves up to J = 53 were required.

Mean Potential Phase Space Theory

The MPPST constitutes a semi-classical statistical approach to tackle the study of atom-diatom reactions.[48, 49] It is based on the same statistical assumptions for the intermediate complex states as the SQM method. However, individual probabilities for the asymptotic semiclassically quantized (v, j, l) states to use in Eq. (1) are calculated in an approximate manner via a two-body capture model[50] including tunneling by means of the WKB model[51] through the radial effective potential obtained by averaging over the reactant γ Jacobi coordinate. Such an averaging allows to implicitly account for the weak anisotropies involved in complex-formation dynamics for barrierless processes at low collision energies. In the present implementation, internal states of both reactant and product channels are computed within the rigid rotor anharmonic oscillator.[49, 52] The isotropic assumption for the inter-fragment potential produces capture cross sections which do not depend on the initial rotational state of the reactant diatom, so only the ground rotational HD (v=0,j=0) state has been taken into account. In the calculation of the rate coefficient 1000 values of the collision energy up to 8 k_B T have been employed.

Ring Polymer Molecular Dynamics

The RPMD method[53] is a very reliable and efficient approach to calculate the thermal rate constant which has been extensively benchmarked over the past few years.[54] This method is based on the isomorphism that exists between a quantum system and its *n*-classical copies (beads) connected to its nearest neighbour through a harmonic potential, forming a necklace in an extended *n*-dimensional phase space. RPMD is not only exact for several static properties (in its short-time limit), but the real-time dynamics of this fictitious ring polymer also provides a reliable estimate for the correlation functions responsible for the thermal rate constant.[54] The computational procedure of RPMD rate calculation is well documented elsewhere[54, 55] and will be not repeated in the present paper. Briefly, along the lines of Bennett-Chandler factorization scheme,[56, 57] the calculation of the RPMD rate constant usually involves the following steps: (1) construction of the ring polymer potential of mean force (PMF), $W(\xi)$ along the reaction coordinate ξ within the confinement of two dividing surfaces and (2) subsequent determination of the ring polymer transmission coefficient or recrossing factor, κ. The recrossing factor ensures that the final RPMD rate constant value is independent of the choice of dividing surfaces and is generally calculated at the maximum of the PMF so as to minimize the propagation time to reach the plateau for κ.

The RPMD rate calculations have been performed over the 1 ^{1}A′ and 1 ^{1}A″ PESs of Dobbyn and Knowles,[46, 47] using the RPMDrate code developed by one of us (Y. Suleymanov).[55] The input parameters of the RPMDrate code have been summarized in Table S1 in the supplementary material. They are very similar to those used in the isotopic variants of the O(^1D) + HD reaction, viz. O(^1D) + H_2[21] and O(^1D) + D_2[22] reactions, except for one dividing surface parameter R_∞ value which has been increased to 60 a_0 to minimize the effect of the long-range electrostatic potential on the rate constant at low temperatures.[58] Consequently, the force constant has also been increased to sample a considerable number of distributions at long

separations. Owing to the computationally expensive nature of the RPMD rate simulations, we determine the RPMD rate constants at the two limiting temperatures (296 K and 50 K) of the experiment. The plots of PMF against ξ are similar to those obtained for the O(^1D) + H_2 and O(^1D) + D_2 reactions (see Figure S3) and illustrate the barrierless complex-forming and thermally activated free energy profile for the 1 ^{1}A′ and 1 ^{1}A″ states respectively. Before entering the complex-forming zone, one can detect small barriers on the PMF profiles of the 1 1A′ PES. The barrier height is greater at 296 K (~ 80 meV) compared to the one at 50 K (~ 14 meV). The existence of these barriers is purely thermodynamic in nature and stems from the decrease in entropy from the reactant side to the intermediate complex-forming zone. The plateau values of κ (see Figure S4) have been attained only after a longer propagation time (1 ps) for the 1 ^{1}A′ PES compared to the 1 ^{1}A″ PES (0.1 ps) and is characteristic of a barrierless reaction with a deep potential well.[54] They show seemingly opposite temperature dependences for these PES's, and the corresponding κ's are very small for the 1 ^{1}A″ state suggesting that the activated complexes will most likely decay back to the reactant channel.

4 Results and Discussion

Reaction dynamics

Indications of the good performance of statistical techniques to reproduce some of the observed features of the title reaction have been shown before.[25] In particular, the DCS for the O(^1D)+HD → OH+D reaction at a 74 meV collision energy calculated by means of the SQM method was found to be in fairly good agreement with results from time dependent wave packet calculations and TOF spectroscopic measurements reported in Ref. (14). Further support for a possible complex-forming mechanism at this energy is provided in the supplementary material. In order to analyse the distinct dynamical mechanisms on each product arrangement of the O(^1D)+HD reaction requires the calculation of both OD+H and OH+D final channels. In this sense, the experimental excitation functions reported by Hsu *et al.*[9] constitute a valuable benchmark. In

Figure 1, we show the SQM and MPPST cross sections for each product channel and the excitation functions from Ref. (9).

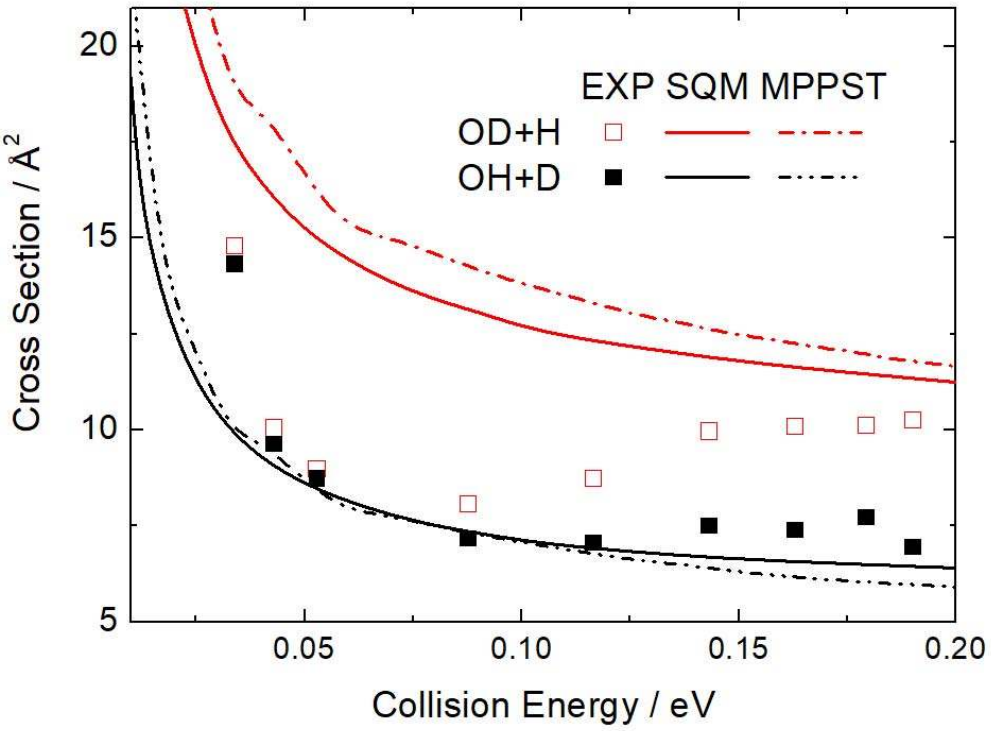

Figure 1. Integral cross sections as a function of the collision energy for both the (black) O(^1D) + HD → OH+D and (red) O(^1D) + HD → OD+H reactions. (Solid lines) SQM results and (dashed dotted lines) MPPST results are compared with (squares) experimental excitation functions from Ref. (9) which have been scaled here to compare with the theoretical predictions in Å^2.

The measured values for the OH forming arrangement, once scaled for comparison with the theoretical predictions, are fairly well described for almost the entire energy range under consideration. The only exception is the excitation function at E_c = 0.033 eV (0.79 kcal mol^{-1}), thus showing that the trend followed by the experimental results in the lowest energy region is not that seen in the statistical results. But the most remarkable disagreement between theory

and experiment regards the distinct ratio between cross sections for the OH and OD forming product arrangements. In particular, measurements by Hsu *et al.*[9] suggest that there are no significant differences between both processes, O(^1D) + HD → OH+D and O(^1D) + HD → OD+H below E_c ≈ 0.1 eV. The σ(OD+H) / σ(OH+D) ratio, not shown here (see Figure 1 (b) of Ref. (9)), remains close to 1 at lower energies and starts to increase beyond 0.1 eV reaching a value of 1.5 at E_c = 0.19 eV (4.42 kcal mol^{-1}). The SQM and MPPST cross sections for the OD+H forming channel, in contrast, are clearly larger than those for the OH+D channel with values for the above mentioned OD/OH ratio which oscillate between 1.6 and 1.7 for SQM (1.85 and 2 for MPPST) for the energy range shown in Figure 1. Thus, experimental and theoretical cross sections for the O(^1D) + HD → OD+H reaction are only close when we approach 0.2 eV collision energy.

In this sense, it is worth mentioning that the 1A´´ PES presents a collinear barrier of 0.1 eV so at higher energies one might expect an increasing contribution coming from the direct reaction mechanism on the excited surface. That would explain the sudden discrepancies arising above 0.15 eV when the experimental excitation function for the OH forming channel is compared with the statistical cross sections. More intriguing are however the differences seen in the similar comparison established for the formation of OD, since, we do not see obvious reasons not to expect a similar good statistical description as for OH+D case, although some previous investigations on the O(^1D) + HCl reaction[60] revealed deviations from statistical predictions obtained by the present SQM approach and its QCT version, the SQCT method reported by Aoiz *et al.* [61], for the OH + Cl product channel but not for the ClO + H product arrangement.

Excitation functions measured by Liu's group for the S(^1D) + HD reaction[62] were different for each product channel SD + H / SH + D for the entire energy range there studied (E_c < 0.3 eV). A comparative dynamics of the two possible product arrangements for the N(^2D) + HD reaction can be found in the investigation by Bañares *et al.*[63] Despite the obvious differences of the

profile for the cross section reported in Ref. (63) (due to the existence of a barrier in the PES for the NH_2 system) with respect to the case studied here, distributions for the ND+H product channel become larger than those for the NH+D as soon as the collision energy starts to increase beyond the reaction threshold (see Figures 2 and 3 from Ref. (63)). This feature is also seen for QCT results included in that work for comparison with the statistical treatment.

Aoiz *et al.*[64] carried out a multisurface QCT investigation of the title reaction and calculated DCSs for different values of the collision energy. In particular, at E_c = 89 meV, where contributions from excited PESs are still very minor, the angular distribution for both product arrangements are fairly well reproduced by statistical means. The comparison with QCT DCSs reported in that work and the present SQM and MPPST predictions is shown in Figure 2.

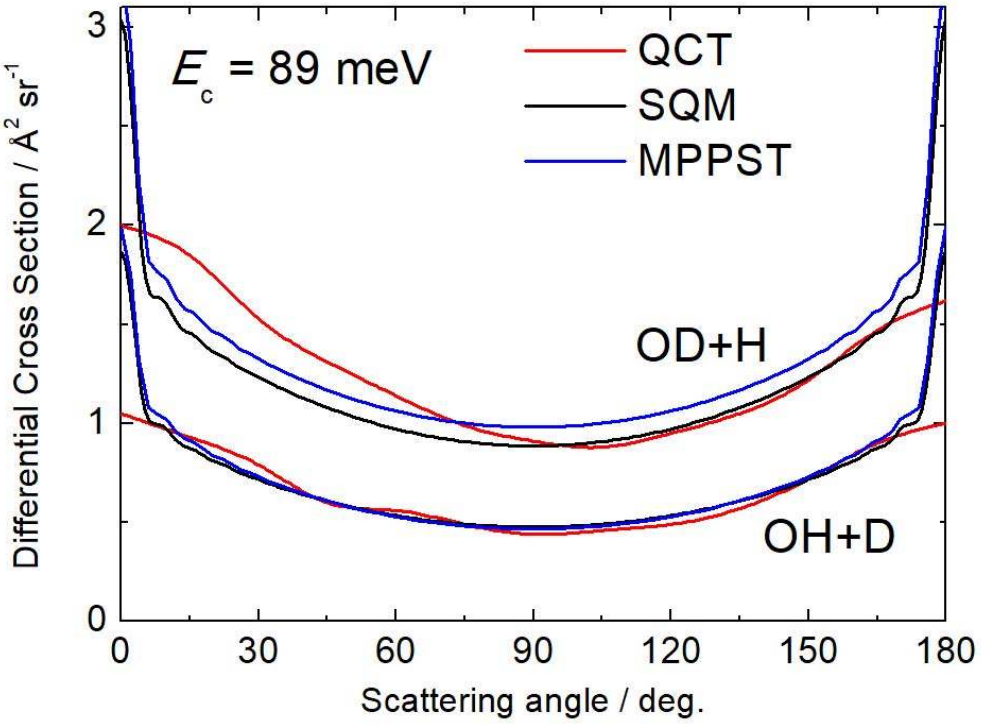

Figure 2. Differential cross sections at 89 meV collision energy for the O(^1D) + HD → OH+D and O(^1D) + HD → OD+H reactions. (Black) SQM results and (blue) MPPST results are compared with (red) QCT results from Ref. (64). Units are Å^2 sr^{-1}.

The agreement is particularly good for the sideways scattering direction (θ ≈ 90 degrees) in the case of the formation of OH. For the other channel, forming OD+H products, the QCT angular distribution exhibits a certain asymmetry which slightly differs from the strict forward-backward symmetry of the statistical result. The complete absence of marked peaks at either θ ≈ 0 and 180 degrees observed in the QCT results which precludes a better accord with the SQM and MPPST predictions can possibly be attributed to parity conservation issues in the classical calculations.[45, 65, 66]

It should be noted that the quantitative differences between SQM and MPPST mainly originate from the way asymptotic diatom states are treated within both approaches. While SQM computes exactly the diatom states on the DK PES, MPPST approximates them using the RRHO model as previously mentioned. This leads to slight differences in the number of available states in reactant/product channels, in particular for the OD+H channel. Small discrepancies may also arise from the mean potential approximation in the MPPST.

As a general conclusion from the above discussed examples, one can suggest that the dynamics of the O(^1D) + HD reaction is close to a complex-forming mechanism for those low and intermediate energies, such as those considered in this work, where reaction over the ground electronic surface dominates. As revealed in previous work, such as the study of Aoiz *et al.*[64] mentioned above, the role played by excited electronic surfaces at larger energies gives rise to asymmetries in the DCSs which are usually understood as indications of an abstraction mechanism.

Experimental Rate Constants

In terms of the kinetic measurements, all the experiments described here were performed under pseudo-first-order conditions using a large excess concentration of HD with respect to O(^1D) atoms. Under these conditions, O(^1D) atoms decayed exponentially as a function of time.

Typical decay profiles of the O(^1D) VUV LIF signal (which is proportional to the O(^1D) concentration) recorded at 127 K are shown in Figure 3.

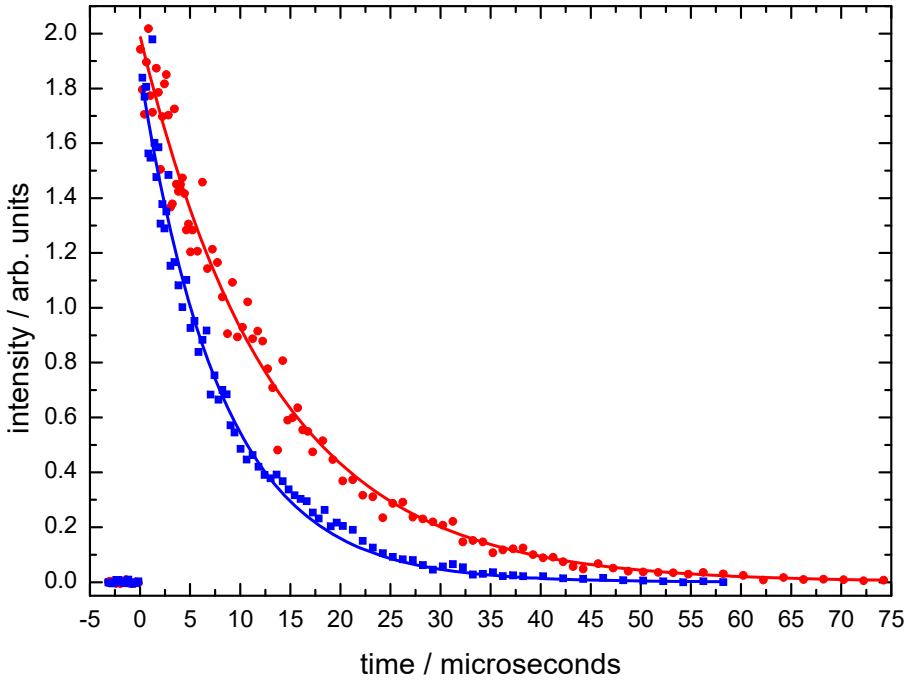

Figure 3. O(^1D) VUV LIF signal as a function of delay time between the photolysis and probe lasers. (Red solid circles) without HD (the O(^1D) VUV LIF signal decays due to quenching collisions with the carrier gas Ar); (blue solid squares) [HD] = 3.4×10^{14} cm^{-3}. Solid lines represent single exponential fits to the individual datasets.

O(^1D) is seen to decay rapidly to zero even in the absence of HD, due to its electronic quenching through collisions with the carrier gas Ar. When HD is added to the flow, the decay rate increases due to reactive removal of O(^1D) atoms by HD. As shown by the solid line fits in Figure 3, these data are well described by a functional form $I_{O(^1D)} = I_{O(^1D)_0} exp(-k't)$ where t is time and $I_{O(^1D)}$ and $I_{O(^1D)_0}$ are the time dependent and initial O(^{1}D) VUV LIF intensities respectively. Values of the pseudo-first-order rate constant, k', were determined for a range of

HD concentrations and in the absence of HD at any given temperature. Then, the values of k' derived in any single experiment were plotted as a function of the corresponding HD concentration as shown in Figure 4 for data recorded at 50 K and 296 K.

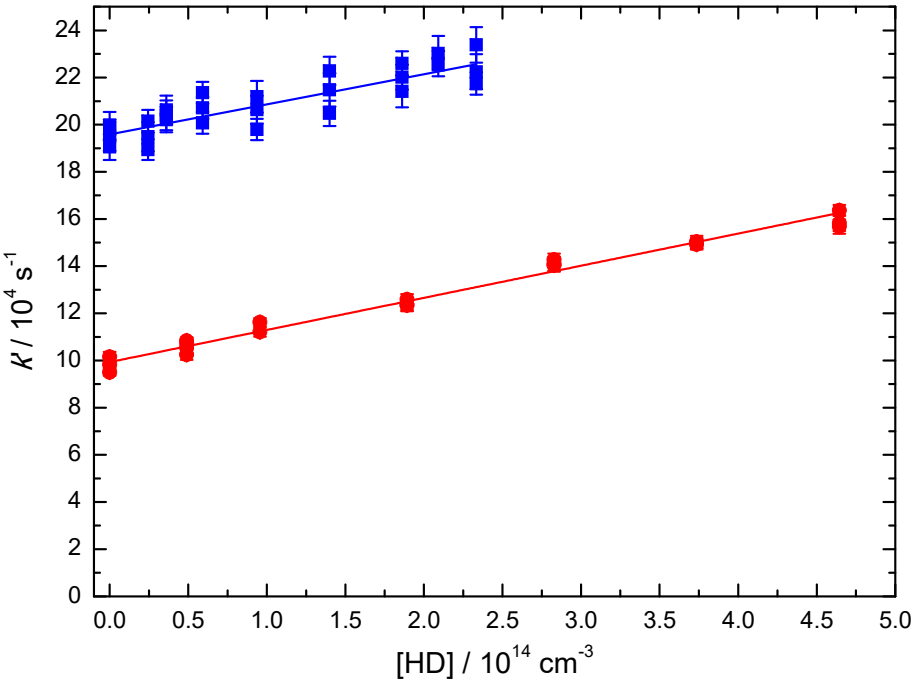

Figure 4. Second-order plots for the O(^1D) + HD reaction. (Red solid circles) data recorded at 296 K; (blue solid squares) data recorded at 50 K. Solid lines represent weighted fits to the individual datasets with statistical uncertainties (1σ) derived from single exponential fits to intensity profiles similar to those shown in Figure 3.

A weighted linear least-squares fit to the individual datasets yielded the second-order rate constant from the slope, with the y-axis intercept value being essentially due to the Ar carrier gas quenching contribution (see Nuñez-Reyes *et al.*[22] and Grondin *et al.*[39] for more details). The measured second-order rate constants are listed in Table 1 alongside other relevant

information and are displayed as a function of temperature in Figure 5 alongside the present theoretical results and earlier work.

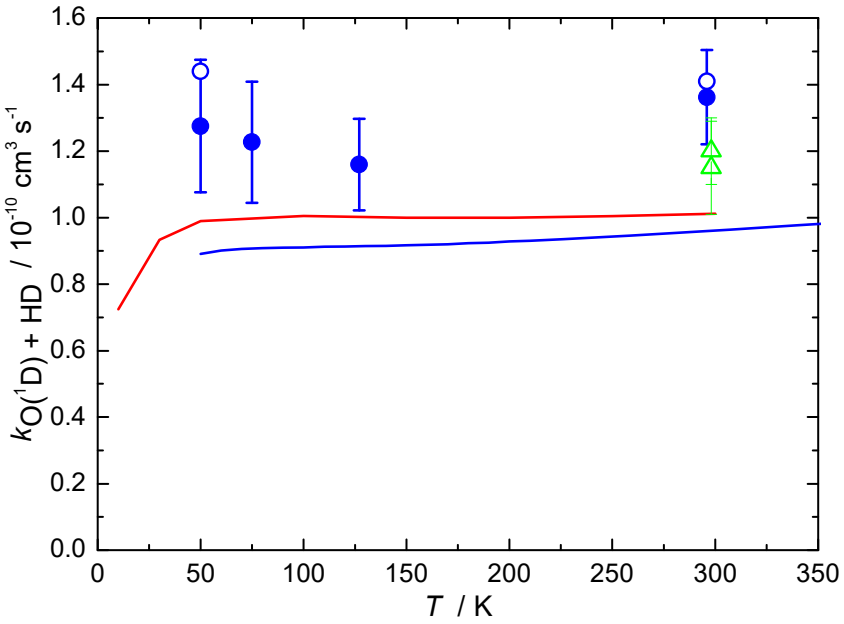

Figure 5. Temperature dependence of the rate constant for the O(^1D) + HD reaction. Experiment: (solid blue circles) this work, O(^1D) VUV LIF detection; (open green triangles) Talukdar and Ravishankara.[16] Theory: (solid red line) this work, MPPST; (solid blue line) this work, SQM; (Open blue circles) this work, RPMD.

Table 1 Measured second-order rate constants for the O(^1D) + HD reaction

T / K	N^b	[HD]/ 10^{14} cm^{-3}	$k_{O(^1D)+HD}$ / 10^{-10} cm^3 s^{-1}
296	21	0 - 4.64	(1.36 ± 0.14)[c]
127 ± 2	21	0 - 3.44	(1.16 ± 0.14)
75 ± 2	20	0 - 1.69	(1.23 ± 0.18)
50 ± 1	27	0 - 2.33	(1.28 ± 0.20)

[a]Uncertainties on the calculated temperatures represent the statistical (1σ) errors obtained from Pitot tube measurements of the impact pressure. [b]Number of individual measurements.

[c]Uncertainties on the measured rate constants represent the combined statistical (1σ) and estimated systematic (10%) errors.

There are surprisingly few earlier kinetic measurements of the rate constant for the O(^1D) + HD reaction and these have only been performed at room temperature. Laurent et al.[7] used the pulsed laser photolysis of N_2O at 193 nm to produce O(^1D) in their experiments. H- or D-atom product formation was followed by VUV LIF around 121.5 nm where the tunable VUV radiation was generated by a resonant sum-difference frequency mixing scheme. They obtained a rate constant equal to $(2.3 \pm 0.4) \times 10^{-10}$ cm^3 s^{-1}, considerably larger than value obtained in the present study of $k_{O(^1D)+HD}$(296 K) = $(1.36 \pm 0.14) \times 10^{-10}$ cm^3 s^{-1}. This difference can be explained by the relatively low pressures of 70 mTorr used by Laurent *et al.*[7] during their experiments, such that the nascent O(^1D) atoms were not thermally equilibrated. In later work, Talukdar & Ravishankara[16] used the pulsed laser photolysis of O_3 at 248 nm as the source of O(^1D) atoms in their work, coupled with resonance fluorescence detection of H(^2S) and O(^3P) production around 121 nm and 130 nm respectively. They derived room temperature rate constants for the O(^1D) + HD reaction equal to $(1.2 \pm 0.1) \times 10^{-10}$ cm^3 s^{-1} and $(1.15 \pm 0.1) \times 10^{-10}$ cm^3 s^{-1}, in good agreement with the value measured in this work. Competing processes such as the electronic quenching of O(^1D) atoms to O(^3P) were estimated to contribute less than 5 % to the overall rate constant. In common with our earlier work on the O(^1D) + H_2 and O(^1D) + D_2 reactions, the rate constants do not vary significantly as a function of temperature within the 50 K to 296 K range, considering the combined errors bars of the present measurements. If we compare the present experimental and theoretical rate constants, it can be seen that the experimental values are approximately 10-20 % larger than the ones determined by the SQM and MPPST methods. Our previous work on the O(^1D) + H_2[21] and O(^1D) + D_2 reactions[22] demonstrated similar discrepancies between the measured and predicted rate constants with the experimental values consistently larger than these theoretical ones. These differences could

arise from several sources which have been discussed previously.[22] As reported by Lin and Guo[67], excited PES may also play a role to the overall dynamics of the O(^1D)+H_2 reaction. In particular, whereas the 1^1A" surface is found to have a negligible contribution, the nonadiabatic 2^1A' pathway may contribute a ≈ 10% to the rate constant over a temperature range extended up to 300 K. Since the dynamics on this excited surface is essentially the same complex-forming mechanism observed for the ground 1^1A' PES[67], one should expect that the inclusion of the statistical rate constant calculated on the 2^1A' surface would lead to a better agreement with the measured values. The overall RPMD thermal rate constants calculated in this work at both 296 K and 50 K are in good agreement with the experimental values, exhibiting very little temperature dependence (see Tables S2 and S3). Concerning the individual channels, the RPMD rate constant for OH + D product formation marginally increases with temperature, while that obtained for OD + H products shows the opposite behaviour. In common with previous work,[21, 22] the RPMD results show that the dominant contribution towards the overall thermal rate constant is due to the $1\ ^1A'$ ground state with an essentially negligible contribution from the $1\ ^1A''$ excited state.

Experimental Product Branching Ratios

In our earlier work on C(^1D) reactions, absolute product branching ratios for H-atom formation were obtained by comparing the intensities of pairs of H-atom formation curves produced by the target and reference reactions, where the H-atom production rate was adjusted to yield curves with similar formation rates. Under these conditions, non-reactive losses of either the minor C(^1D) reagent species (such as through quenching with the carrier gas Ar) or the H-atom product (through diffusion) did not affect the measured branching ratios as the contributions of both of these processes were small compared to the reactive loss of C(^1D) atoms. Unfortunately, the O(^1D) + Ar $\rightarrow$ O(^3P) + Ar quenching reaction is much more efficient than the equivalent

process for C(^1D) atoms.[59] Consequently, any small discrepancies in the H-atom formation rates for the target and reference reactions could lead to significantly different non-reactive losses for O(^1D) atoms. This in turn could induce large errors in the H-atom yield measurements for the O(^1D) atom reactions. An alternative method for the determination of absolute branching ratios was recently described by Nuñez-Reyes *et al.*[37] allowing these authors to circumvent the problem. In common with earlier work, the production of H (or D) atoms from the target O(^1D) + HD reaction was measured relative to the reference O(^1D) + H_2 (D_2) reaction which is considered to produce H (or D) atoms with a 100 % yield. In this case, the experiments measured the peak H or D atom VUV LIF signal, I_{max}, for a range of coreagent concentrations for both the target and reference reactions. The time corresponding to the peak intensity, t_{max}, representing the delay between photolysis and probe lasers was calculated prior to the experiments using the expression

$$t_{max} = \frac{1}{k_{L(H)} - k'} \ln\left(\frac{k_{L(H)}}{k'}\right)$$

where k' values were obtained through the kinetic experiments described above following O(^1D) loss, while $k_{L(H)}$, the diffusional loss rate for H (or D) atoms, was obtained from previous H (D) atom detection experiments performed under similar conditions. Typical plots of I_{max} versus t_{max} recorded at 127 K for the target and reference reactions are shown in Figure 6 and can be seen to yield straight lines.

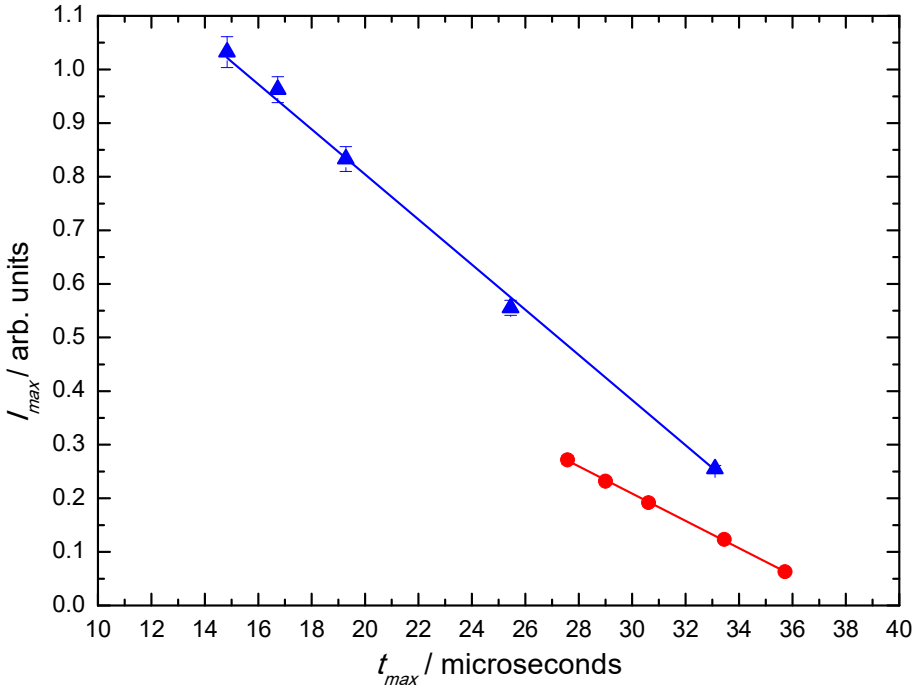

Figure 6. Maximum intensity, I_{max}, as a function of the maximum time, t_{max}, at 127 K; (blue triangles) reference O(^1D) + H_2 reaction; (red circles) target O(^1D) + HD reaction. Solid lines represent weighted fits to the individual data based on the standard error derived from an average of the laser shots recorded at each value of t_{max}.

The slopes of these plots were obtained from weighted linear least-squares fits to the data, where the weighting parameter corresponded to the standard error of the measured intensity. As neither HD nor H_2 (D_2) absorb to any significant extent around 121 nm, no corrections to the relative intensities were required to account for absorption losses. Following the analysis provided by Nuñez-Reyes *et al.*,[37] the absolute H- or D-atom yields were finally obtained from the ratio of the slopes of the two plots. In order to reduce the scope for potential errors in the measured yields (such as through signal drift with time), this procedure was repeated at least five times, while the acquisition order was inverted for each pair of measurements. The absolute

yields of H-(D-) atoms were converted to branching ratios (BR) using the formula BR = X/(1-X) where X is the measured H- or D- atom yield. The derived branching ratios are reported in Table 2 and are displayed as a function of temperature in Figure 7 alongside the present theoretical work in addition to previous experimental and theoretical results.

Table 2 Temperature dependent experimental branching ratios (OD + H/OH + D) for the O(^1D) + HD reaction

T / K	N^a	Branching ratio H(^2S)-detection	N^a	Branching ratio D(^2S)-detection
296	5	1.17 ± 0.20[b]		
127±2[c]	8	1.46 ± 0.11	5	1.09 ± 0.23
75±2	5	1.15 ± 0.23		
50±1	5	1.33 ± 0.13		

[a]Number of branching ratios determinations. [b]The error bars reflect the statistical uncertainties at the 95% confidence level. [c]Uncertainties on the calculated temperatures represent the statistical (1σ) errors obtained from Pitot tube measurements of the impact pressure.

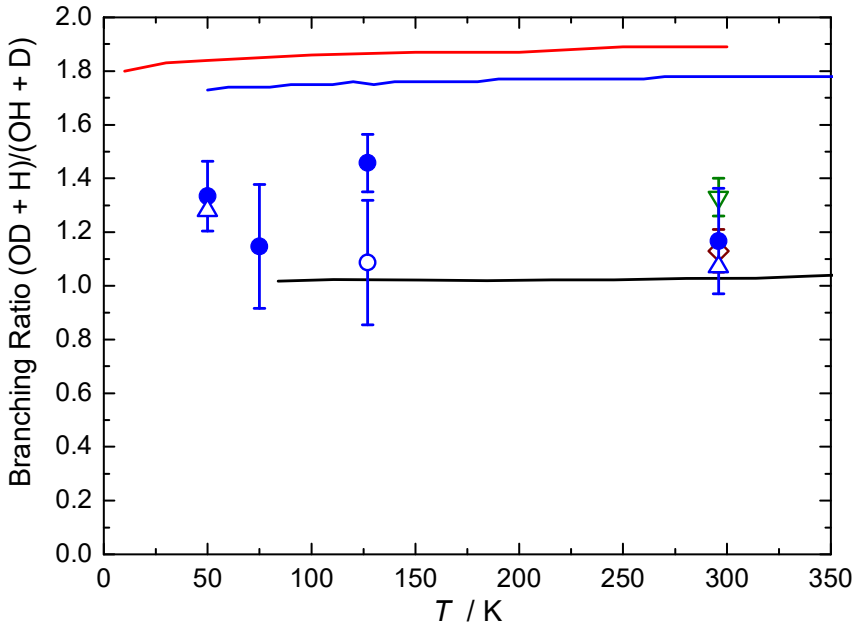

Figure 7. Temperature dependence of the isotopic branching ratio for the O(^1D) + HD reaction. Experiment; (solid blue circles) this work, H-atom detection; (open blue circle) this work, D-atom detection; (inverted open green triangle) Talukdar & Ravishankara;[16] (open red diamond)

Tsukiyama et al.;[4] (solid black line) Hsu et al.[9] Theory; (solid red line) this work, MPPST; (solid blue line) this work, SQM; (Open blue triangles) this work, RPMD.

The present experimental branching ratios are quite scattered compared to the equivalent quantities obtained during previous work on the C(^1D) + HD reaction[34] which employed a simpler method for the determination of branching ratios as described above. Indeed, as only a limited quantity of coreagent HD was available for all the combined experiments reported here (7 litres), it was not possible to use large HD flows during this study. Consequently, the range of t_{max} values that could be adopted for the O(^1D) + HD reaction was restricted as can be seen from Figure 6, leading to higher inaccuracies on the determination of the slope for the target reaction than those for the reference reaction. Nevertheless, it can be seen that the branching ratios obtained here and those derived by previous studies at room temperature are in good agreement, displaying a slight preference for the OD + H product channel over the OH + D one. Earlier measurements[5-8] at higher equivalent energies also yielded (OD + H)/(OH + D) branching ratios in the range 1.1-1.5. Below room temperature, the branching ratio remains relatively constant, considering the experimental error bars, and agrees well with the only other previous measurement of the temperature (energy) dependent branching ratio by Hsu et al.[9] through crossed molecular beam experiments over the energy range 2.5 – 25 kJ mol^{-1}. Although the majority of the present branching ratio measurements were performed by following the H-atom production channel, a limited number of experiments was also performed at 127 K by following D-atom formation (by comparing with the D-atom yield of the O(^1D) + D_2 reaction). These supplementary measurements confirm the overall trend of the branching ratio as a function of temperature.

Interestingly, the MPPST and SQM methods lead to calculated branching ratios that are somewhat larger than the present and previous experimental results, whereas the RPMD

branching ratio shows only a slight preference for OD + H product formation which increases slightly at low temperature. In principle, the overestimation of the experimental branching ratios with respect to the statistical predictions can be attributed to deviations from strict complex-forming dynamics of the OD production channel. This would be consistent, on the other hand, with the comparison shown in Figure 1 between SQM and MPPST cross sections and those from the experiment of Ref. (9), where the statistical results were clearly larger for the OD + H product channel.

In order to check for possible dynamical effects, QCT calculations were carried out using a standard approach[66] for collision energies of 6.5, 19.5 and 39 meV, corresponding to the thermal average collision energies for 50, 150 and 300K and j_{HD}=0. The predicted branching ratios are respectively 1.74, 2.03 and 2.17. While these values are consistent with previous calculations at higher collision energies[64], they do not improve the agreement with experiments. Consequently, it does not seem that the disagreement between the statistical and experimental results stems from classical dynamical effects on the DK 1A′ adiabatic electronic state.

5 Conclusions

We have presented a combined experimental and theoretical investigation of the dynamics and kinetics of the O(^1D) + HD reaction. On the one hand, rate constants between 50 and 300 K were measured with a supersonic flow apparatus employing laser photolysis and laser induced fluorescence to produce and detect O(^1D), respectively. Branching ratios (OD+H / OH+D) were additionally obtained by comparison with a reference reaction by following H(^2S) or D(^2S) production. On the other hand, theoretical estimates for the thermal rate constants have been calculated using mean potential phase space theory, statistical quantum method and ring polymer molecular dynamics. The comparison between experiment and theory reveals a reasonably good agreement with some slightly larger deviations observed for the statistically

based predictions. The role played by complex-forming mechanisms in the overall dynamics for the processes leading to the formation of either OD or OH is further investigated by comparison with previously reported integral and differential cross sections for each product arrangement.

Supporting Information. Supplemental discussion of the reaction dynamics. Supplemental figures S1-S4. Supplemental tables S1-S3.

Acknowledgments

TGL acknowledges support from MICINN with Grant FIS2017-83157-P and help from Aurora Nogales to adapt some of the numerical data from the literature. KMH acknowledges support from the French programs “Physique et Chimie du Milieu Interstellaire” (PCMI) and "Programme National de Planétologie" (PNP) funded by the Centre National de la Recherche Scientifique (CNRS) and Centre National d’Etudes Spatiales (CNES). Y.V.S. acknowledges the support of the European Regional Development Fund and the Republic of Cyprus through the Research Promotion Foundation (Project: INFRASTRUCTURE/1216/0070). Computer time was provided by the Pôle Modélisation HPC facilities of the Institut des Sciences Moléculaires UMR 5255 CNRS − Université de Bordeaux, co-funded by the Nouvelle Aquitaine region.

References

(1) Sander, S. P.; J. Abbatt; J. R. Barker; J. B. Burkholder; R. R. Friedl; D. M. Golden; R. E. Huie; C. E. Kolb; M. J. Kurylo; G. K. Moortgat; V. L. Orkin; Wine, P. H., Chemical Kinetics and Photochemical Data for Use in Atmospheric Studies, Evaluation No. 17. *JPL Publication 10-6, Jet Propulsion Laboratory, Pasadena, 2011* http://jpldataeval.jpl.nasa.gov/. **2011**.

(2) Schmidt, J. A.; Johnson, M. S.; Schinke, R. Carbon Dioxide Photolysis from 150 to 210 nm: Singlet and Triplet Channel Dynamics, UV-spectrum, and Isotope Effects. *Proc. Natl. Acad. Sci. U. S. A.* **2013**, *110*, 17691-17696.

(3) Nair, H.; Allen, M.; Anbar, A. D.; Yung, Y. L. A Photochemical Model of the Martian Atmosphere. *Icarus* **1994**, *111,* 124-150.

(4) Tsukiyama, K.; Katz, B.; Bersohn, R. Isotopic Branching Ratio for the Reaction A +HD → AD(H) + H(D). *J. Chem. Phys.* **1985**, *83*, 2889-2893.

(5) Butler, J. E.; Jursich, G. M.; Watson, I. A.; Wiesenfeld, J. R. Reaction Dynamics of O($^1D_2$)+H_2, HD, D_2: OH, OD ($X^2\Pi$) Product Internal Distributions. *J. Chem. Phys.* **1986**, *84*, 5365-5377.

(6) Matsumi, Y.; Tonokura, K.; Kawasaki, M.; Kim, H. L. Dynamics of the Reaction O(^1D)+HD, H_2 and D_2: Isotopic Branching Ratios and Translational Energy Release. *J. Phys. Chem.* **1992**, *96***,** 10622-10626.

(7) Laurent, T.; Naik, P. D.; Volpp, H.-R.; Wolfrum, J.; Arusi-Parpar, T.; Bar, I.; Rosenwaks, S. Absolute Rate Constants, Reactive Cross-sections and Isotopic Branching Ratio for the Reaction of O(^1D) with HD. *Chem. Phys. Lett.* **1995**, *236*, 343-349.

(8) Che, D. C.; Liu, K. Reactive Scattering of O(^1D)+HD: Product Speed and Angle Distributions. *J. Chem. Phys.* **1995**, *103*, 5164-5167.

(9) Hsu, Y.-T.; Wang, J.-H.; Liu, K. Reaction Dynamics of O(^1D)+H_2, D_2, and HD: Direct Evidence for the Elusive Abstraction Pathway and the Estimation of its Branching. *J. Chem. Phys.* **1997**, *107***,** 2351-2356.

(10) Hsu, Y.-T.; Liu, K. Product State(s)-Resolved Differential Cross Section of the Reaction O(^1D)+HD → OH(v,j)+D. *J. Chem. Phys.* **1997**, *107,* 1664-1667.

(11) Hsu, Y.-T.; Liu, K.; Pederson, L. A.; Schatz, G. Reaction Dynamics of O(^1D)+HD. I. The Insertion Pathway. *J. Chem. Phys.* **1999**, *111***,** 7921-7930.

(12) Hsu, Y.-T.; Liu, K.; Pederson, L. A.; Schatz, G. Reaction Dynamics of O(^1D)+HD. II. Effects of Excited Surfaces. *J. Chem. Phys.* **1999**, *111*, 7931-7944.

(13) Liu, X.; Lin, J. J.; Harich, S. A.; Yang, X. Quantum State Specific Dynamics for the O(^1D)+HD → OD + H Reaction. *J. Chem. Phys.* **2000**, *113*, 1325-1328.

(14) Yuan, K.; Cheng, Y.; Liu, X.; Harich, S.; Yang, X.; Zhang, D. H. Experimental and Quantum Dynamical Study on an Asymmetric Insertion Reaction: State-to-state Dynamics of O(^1D)+HD($^1\Sigma_g^+$, *v'*=0, *j'*=0) → OH($^2\Pi$, *v''*, *N''*) + D(^{2}S) *Phys. Rev. Lett.* **2006**, *96*, 103202.

(15) Muckerman, J. T. Applications of Classical Trajectory Techniques to Reactive Scattering, in H. Eyring, D. Henderson (Eds.) *Theoretical Chemistry, Advances and Perspectives, Academic Press, New York* **1981**, *6A*, 1-79.

(16) Talukdar, R. K.; Ravishankara, A. R. Rate Coefficients for O(^1D) + H_2, D_2, HD Reactions and H atom Yield in O(^1D) + HD Reaction, *Chem. Phys. Lett.* **1996,** *253*, 177-183.

(17) Fitzcharles, M. S.; Schatz, G. C. A Theoretical Study of Complex Formation, Isotope Effects and Energy Partitioning of the O(^1D) + H_2 (D_2, HD) Reaction *J. Phys. Chem.* **1986**, *90*, 3634-3644.

(18) Schatz, G. C.; Papaioannou, A.; Pederson, L. A.; Harding, L. B.; Hollebeek, T.; Ho, T.-S.; Rabitz, H. A Global A-state Potential Surface for H_2O: Influence of Excited States on the O(^1D)+H_2 Reaction *J. Chem. Phys.* **1997**, *107*, 2340-2350.

(19) Alagia, M.; Balucani, N.; Cartechini, L.; Casavecchia, P.; van Kleef, E. H.; Volpi, G. G.; Kuntz, P. J.; Sloan, J. J. Crossed Molecular Beams and Quasiclassical Trajectory Studies of the Reaction O(^1D)+H_2(D_2). *J. Chem. Phys.* **1998**, *108*, 6698-6708.

(20) Aoiz, F. J.; Bañares, L.; Herrero, V. J. A Theoretical Study of the Dynamics of the O(^1D)+HD Reaction at 0.196 eV Collision Energy: Comparison with Experimental Results, *Chem. Phys. Lett.* **1999**, *310*, 277-286.

(21) Hickson K. M.; Suleimanov, Y. V. Low-Temperature Experimental and Theoretical Rate Constants for the O(^1D) + H_2 Reaction. *J. Phys. Chem. A* **2017**, *121*, 1916-1923.

(22) Nuñez-Reyes, D.; Hickson, K. M.; Larrégaray, P.; Bonnet, L.; González-Lezana T.; Suleimanov, Y. V. A Combined Theoretical and Experimental Investigation of the Kinetics and Dynamics of the O(^1D)+D_2 Reaction at Low Temperature, *Phys. Chem. Chem. Phys.* **2018***, 20*, 4404-4414.

(23) Rivero-Santamaría, A.; González-Martínez, M. L.; González-Lezana, T.; Rubayo-Soneira, J.; Bonnet, L.; Larrégaray, P. The O(^1D) + H_2 (X $^1\sum^+$, v,j) → OH(X $^2\Pi$, v',j') + H(^2S) Reaction at Low Collision Energy: When a Simple Statistical Description of the Dynamics Works. *Phys. Chem. Chem. Phys.* **2011***, 13*, 8136-8139.

(24) Rackham, E. J.; González-Lezana, T.; Manolopoulos, D. E. A Rigorous Test of the Statistical Model for Atom-Diatom Insertion Reactions. *J. Chem. Phys.* **2003**, *119,* 12895-12907.

(25) González-Lezana, T. Statistical Quantum Studies on Insertion Reactions, *Int. Rev. Phys. Chem.* **2007***, 26*, 29-91

(26) Daugey, N.; Caubet, P.; Retail, B.; Costes, M.; Bergeat, A.; Dorthe, G., Kinetic Measurements on Methylidyne Radical Reactions with Several Hydrocarbons at Low Temperatures. *Phys. Chem. Chem. Phys.* **2005,** *7*, 2921-2927.

(27) Daugey, N.; Caubet, P.; Bergeat, A.; Costes, M.; Hickson, K. M., Reaction Kinetics to Low Temperatures. Dicarbon + Acetylene, Methylacetylene, Allene and Propene from 77 ≤ T ≤ 296 K. *Phys. Chem. Chem. Phys.* **2008,** *10*, 729-737.

(28) Hickson, K. M.; Loison, J.-C.; Guo, H.; Suleimanov, Y. V., Ring-Polymer Molecular Dynamics for the Prediction of Low-Temperature Rates: An Investigation of the C(^1D) + H_2 Reaction. *J. Phys. Chem. Lett.* **2015,** *6*, 4194-4199.

(29) Hickson, K. M.; Suleimanov, Y. V., An Experimental and Theoretical Investigation of the C(^1D) + D_2 Reaction. *Phys. Chem. Chem. Phys.* **2017**, *19*, 480-486.

(30) Nuñez-Reyes, D.; Hickson, K. M., Kinetic and Product Study of the Reactions of C(^1D) with CH_4 and C_2H_6 at Low Temperature. *J. Phys. Chem. A* **2017,** *121*, 3851-3857.

(31) Nuñez-Reyes, D.; Hickson, K. M., The Reactivity of C(^1D) with Oxygen Bearing Molecules NO and O_2 at Low Temperature. *Chem. Phys. Lett.* **2017,** *687*, 330-335.

(32) Hickson, K. M.; Loison, J.-C.; Lique, F.; Kłos, J., An Experimental and Theoretical Investigation of the C(^1D) + N_2 → C(^3P) + N_2 Quenching Reaction at Low Temperature. *J. Phys. Chem. A* **2016,** *120*, 2504-2513.

(33) Nuñez-Reyes, D.; Hickson, K. M., Kinetics of the Gas-Phase O(^1D) + CO_2 and C(^1D) + CO_2 Reactions over the 50–296 K Range. *J. Phys. Chem. A* **2018,** *122*, 4002-4008.

(34) Wu, Y.; Cao, J.; Ma, H.; Zhang, C.; Bian, W.; Nuñez-Reyes, D.; Hickson, K. M., Conical-Intersection Regulated Intermediates in Bimolecular Reactions: Insights from C(^1D) + HD Dynamics. *Sci. Adv*. **2019**, *5*, eaaw0446.

(35) Nuñez-Reyes, D.; Hickson, K. M., A Low Temperature Investigation of the Gas-Phase N(^2D) + NO Reaction. Towards a Viable Source of N(^2D) Atoms for Kinetic Studies in Astrochemistry. *Phys. Chem. Chem. Phys.* **2018,** *20*, 17442-17447.

(36) Meng, Q. Y.; Hickson, K. M.; Shao, K. J.; Loison, J. C.; Zhang, D. H., Theoretical and Experimental Investigations of Rate Coefficients of O(^1D) + CH_4 at Low Temperature. *Phys. Chem. Chem. Phys.* **2016,** *18*, 29286-29292

(37) Nuñez-Reyes, D.; Hickson, K. M., Rate Constants and H-Atom Product Yields for the Reactions of O(^1D) Atoms with Ethane and Acetylene from 50 to 296 K. *J. Phys. Chem. A* **2018,** *122*, 4696-4703.

(38) Nuñez-Reyes, D.; Kłos, J.; Alexander, M. H.; Dagdigian, P. J.; Hickson, K. M., Experimental and Theoretical Investigation of the Temperature Dependent Electronic Quenching of O(^1D) Atoms in Collisions with Kr. *J. Chem. Phys.* **2018,** *148*, 124311.

(39) Grondin, R.; Loison, J.-C.; Hickson, K. M., Low Temperature Rate Constants for the Reactions of O(^1D) with N_2, O_2, and Ar. *J. Phys. Chem. A* **2016,** *120*, 4838-4844.

(40) Streit, G. E.; Howard, C. J.; Schmeltekopf, A. L.; Davidson, J. A.; Schiff, H. I., Temperature Dependence of O(^1D) Rate Constants for Reactions with O_2, N_2, CO_2, O_3, and H_2O. *J. Chem. Phys.* **1976,** *65*, 4761-4764.

(41) Davidson, J. A.; Schiff, H. I.; Brown, T. J.; Streit, G. E.; Howard, C. J., Rate Constants for the Deactivation of O(^1D) by Xe, Kr, and Ar over the Range 110–330 K. *J. Chem. Phys.* **1978,** *69*, 1213-1215.

(42) Hilbig, R.; Wallenstein, R., Enhanced Production of Tunable VUV Radiation by Phase-Matched Frequency Tripling in Krypton and Xenon. *Quantum Electronics, IEEE Journal of* **1981,** *17*, 1566-1573.

(43) Bargueño, P.; González-Lezana, T.; Larrégaray, P.; Bonnet, L.; Rayez, J.-C. Time Dependent Wave Packet and Statistical Calculations on the H+O_2 Reaction, *Phys. Chem. Chem. Phys.* **2007**, *9*, 1127-1137.

(44) Bargueño, P.; González-Lezana, T.; Larrégaray, P.; Bonnet, L.; Rayez, J.-C.; Hankel, M.; Smith, S. C.; Meijer, A. J. H. M. Study of the H+O_2 Reaction by Means of Quantum Mechanical and Statistical Approaches: The Dynamics on Two Different Potential Energy Surfaces, *J. Chem. Phys.* **2008***, 128*, 244308.

(45) Bonnet, L.; Larrégaray, P.; Rayez, J.-C.; González-Lezana, T. Parity Conservation and Polarization of Differential Cross Sections in Complex-forming Chemical Reactions, *Phys. Chem. Chem. Phys.* **2006***, 8*, 3951-3954.

(46) Dobbyn, A. J.; Knowles, P. J. A Comparative Study of Methods for Describing Non-Adiabatic Coupling: Diabatic Representation of the $^1\sum^+/^1\Pi$ HOH and HHO Conical Intersections *Mol. Phys.* **1997**, *91*, 1107-1124.

(47) Dobbyn, A. J.; Knowles, P. J. General Discussion. *Farad. Discuss.* **1998**, *110*, 247.

(48) Larrégaray, P.; Bonnet, L.; Rayez, J.-C. Mean Potential Phase Space Theory of Chemical Reactions *J. Chem. Phys.* **2007***, 127*, 084308

(49) Larrégaray, P.; Bonnet, L.; Rayez, J.-C. Validity of Phase Space Theory for Atom-Diatom Insertion Reactions *J. Phys. Chem. A* **2006**, *110*, 1552-1560

(50) Langevin, P. Une Formule Fondamentale de Théorie Cinétique. *Ann. Chim. Phys.* **1905**, *5*, 245-288.

(51) Meana-Paneda, R.; Truhlar, D. G.; Fernández-Ramos, A. Least-Action Tunneling Transmission Coefficient for Polyatomic Reactions. *J. Chem. Theory Comput.* **2010**, *6*, 6-17.

(52) *NIST Chemistry WebBook, NIST Standard Reference Database Number 69*, edited by P. J. Linstrom and W. G. Mallard (National Institute of Standards and Technology, Gaithersburg, MD, 2017).

(53) Habershon, S.; Manolopoulos, D. E.; Markland, T. E.; Miller III, T. F. Ring-Polymer Molecular Dynamics: Quantum Effects in Chemical Dynamics from Classical Trajectories in an Extended Phase Space, *Annu. Rev. Phys. Chem.* **2013**, *64*, 387-413.

(54) Suleimanov, Y. V.; Aoiz, F. J.; Guo, H. Chemical Reaction Rate Coefficients from Ring Polymer Molecular Dynamics: Theory and Practical Applications, *J. Phys. Chem. A* **2016**, *120*, 8488-8502.

(55) Suleimanov, Y. V.; Allen, J. W.; Green, W. H. RPMDrate: Bimolecular Chemical Reaction Rates from Ring Polymer Molecular Dynamics, *Comput. Phys. Commun.* **2013**, *184*, 833-840.

(56) Bennett, C. H. *Algorithms for Chemical Computations*, edited by R. E. Christofferson, (ACS Symposium Series No. 46, American Chemical Society, Washington, DC, 1977).

(57) Chandler, D. Statistical Mechanics of Isomerization Dynamics in Liquids and the Transition State Approximation, *J. Chem. Phys.* **1978**, *68*, 2959-2970.

(58) Bhowmick, S.; Bossion, D.; Scribano, Y.; Suleimanov, Y. V. The Low Temperature $D^+ + H_2 \rightarrow HD + H^+$ Reaction Rate Coefficient: a Ring Polymer Molecular Dynamics and Quasi-classical Trajectory Study, *Phys. Chem. Chem. Phys.* **2018**, *20*, 26752-26763.

(59) Husain, D.; Kirsch, L. J. Study of Electronically Excited Carbon Atoms, $C(2^1D_2)$, by the Attenuation of Atomic Emission, $(3^1P_1^\circ \rightarrow 2^1D_2)$. Part 1.-Collisional Deactivation of $C(2^1D_2)$ by the Noble Gases. *Trans. Faraday Soc.* **1971,** *67*, 2886-2895.

(60) Bargueño, P.; Jambrina, P. G. and Alvariño, J.M., Menéndez, M., Verdasco, E., Hankel, M., Smith S. C.; Aoiz, F. J. and González-Lezana T. Energy Dependent Dynamics of the $O(^1D)$ + HCl Reaction: A Quantum, Quasiclassical and Statistical Study *Phys. Chem. Chem. Phys.* **2011**, *290*, 8502-8514.

(61) Aoiz, F. J.; González-Lezana, T. and Saéz Rábanos V. A Comparison of Quantum and Quasiclassical Statistical Models for Reactions of Electronically Excited Atoms with Molecular Hydrogen *J. Chem. Phys.* **2008**, *129*, 094305.

(62) Lee, S. H.; Liu, K. Isotope Effects and Excitation Functions for the Reactions of $S(^1D)+H_2$, D_2 and HD. *Chem. Phys. Lett.* **1998**, *290*, 323-328.

(63) Bañares, L.; Aoiz, F. J.; González-Lezana, T.; Herrero, V. J.; Tanarro, I. Influence of Rotation and Isotope Effects on the Dynamics of the $N(^2D)+H_2$ Reactive System and of its Deuterated Variants. *J. Chem. Phys.* **2005**, *123*, 224301.

(64) Aoiz, F. J.; Bañares, L.; Brouard, M.; Castillo, F. J.; Herrero, V. J. The Dynamics of the $O(^1D)$+HD Reaction: A Quasiclassical Trajectory Multisurface Study. *J. Chem. Phys.* **2000**, *113,* 5339-5353.

(65) Bonnet, L.; Larrégaray, P.; Rayez, J.-C. On the Theory of Complex-forming Chemical Reactions: Effect of Parity Conservation on the Polarization of Differential Cross Sections. *Phys. Chem. Chem. Phys.*, **2007**, *9*, 3228–3240.

(66) Bonnet, L. Classical Dynamics of Chemical Reactions in a Quantum Spirit, *Int. Rev. Phys. Chem*. **2013**, *32*, 171-228.

(67) Lin, S. Y. and Guo, H. Adiabatic and Nonadiabatic State-to-State Quantum Dynamics for $O(^1D)+H_2$ ($X^1\Sigma_g^+$, v_i, $j_i = 0$) → $OH(X^2\,\Pi, v_f, j_f)+H(^2S)$ Reaction *J. Phys. Chem. A* **2009**, *113*, 4285-4293.